Annals of Glaciology 59(77) 2018 doi: 10.1017/aog.2018.20

Characteristics and sources of dissolved organic matter in a glacier in the northern Tibetan Plateau: differences between different snow categories

Lin FENG,[1,2] Yanqing AN,[1] Jianzhong XU,[1] Shichang KANG[1,3]

[1]*State Key Laboratory of Cryospheric Science, Northwest Institute of Eco-Environment and Resources, Chinese Academy of Sciences (CAS), Lanzhou 730000, China.*
E-mail: jzxu@lzb.ac.cn
[2]*University of Chinese Academy of Sciences, Beijing 100049, China*
[3]*CAS Center for Excellence in Tibetan Plateau Earth Sciences, Beijing 100101, China*

ABSTRACT. Dissolved organic matter (DOM) in mountain glaciers is an important source of carbon for downstream aquatic systems, and its impact is expected to increase due to the increased melting rate of glaciers. We present a comprehensive study of Laohugou glacier no. 12 (LHG) at the northern edge of the Tibetan Plateau to characterize the DOM composition and sources by analyzing surface fresh snow, granular ice samples, and snow pit samples which covered a whole year cycle of 2014/15. Excitation–emission matrix fluorescence spectroscopy analysis of the DOM with parallel factor analysis (EEM-PARAFAC) identified four components, including a microbially humic-like component (C1), two protein-like components (C2 and C3) and a terrestrial humic-like component (C4). The use of Fourier transform ion cyclotron resonance mass spectrometry (FT-ICR MS) showed that DOM from all these samples was dominated by CHO and CHON molecular formulas, mainly corresponding to lipids and aliphatic/proteins compounds, reflecting the presence of significant amounts of microbially derived and/or deposited biogenic DOM. The molecular compositions of DOM showed more CHON compounds in granular ice than in fresh snow, likely suggesting newly formed DOM from microbes during snowmelting.

KEYWORDS: biogeochemistry, glacier chemistry, mountain glaciers

INTRODUCTION

The continuing rapid retreat of glaciers and ice sheets is one of the most prominent signs of climate change (Stocker and others, 2013). With the rapid shrinkage of glaciers, increased glacial meltwater runoff has become an important contributor to downstream water ecosystems (Huss, 2011). Hood and others (2015) estimate that the global-scale glacier storage is ~6 Pg of organic carbon, most of which (77%) is in the form of dissolved organic carbon (DOC), and 15.34 Tg of DOC (0.43 Tg C yr^{-1}) is expected to be liberated from glacier storage by 2050 with the majority (9.68 Tg, or 63%) coming from mountain glaciers. Due to the cascading impacts on nutrient and carbon cycle of downstream systems, the biogeochemical effects of glacial meltwater runoff have received increasing attention (Milner and others, 2017).

Mountain glaciers are well developed in western China, with a total area of 43 087 km^2 based on the results of the second Chinese glacier inventory (Guo and others, 2015). Liu and others (2016) estimated DOC release rates from Chinese mountain glaciers was up to 15.4 ± 6.1 Gg yr^{-1}. High bioavailability of DOC was found in glacier runoff in western China (Spencer and others, 2014). For example, Yan and others (2016) found that the bioavailability of DOC in surface snow samples from Laohugou glacier no. 12 (LHG) on the northern Tibetan Plateau (TP) was 46.2% of the total DOC concentration. Feng and others (2016) revealed the fingerprint of microbially derived dissolved organic matter (DOM) in cryoconite sampled from the ablation zone of LHG, and suggested that fresh snow and granular ice on the surface of TP glaciers could contain autochthonous DOM produced by an in situ microbial process. However, the composition and sources of DOM in snow samples in this region are still poorly understood. In this study, we attempt to investigate the DOM composition and source in connection with snowmelting processes, based on the collection and analysis different categories of snow samples in LHG.

MATERIALS AND METHODS

Sites and sampling

LHG (39.42° N, 96.55° E; 4260–5483 m a.s.l.; Fig. 1) is the largest valley glacier (9.85 km, 20.4 km^2) in the Qilian Mountains at the northern TP. The altitude of the main peak, Daxueshan, is 5483 m. The glacier is the main water source for the Shule River which is the second river in the Hexi Corridor of Gansu province. Climate at LHG is dominated by the East Asian monsoon in summer, and westerlies in winter. Precipitation from May to September accounts for ~70% of the annual total (~350 mm) and is mainly influenced by the East Asian monsoon (Li and others, 2012). The average annual temperature recorded by automatic weather station is ~−6 °C at the glacier terminus (Xu and others, 2013). Arid and semiarid regions surround this region, with Tarim Basin (Taklimakan Desert) to the west, Qaidam Basin to the southwest, and the Gobi Desert to the

https://doi.org/10.1017/aog.2018.20 Published online by Cambridge University Press

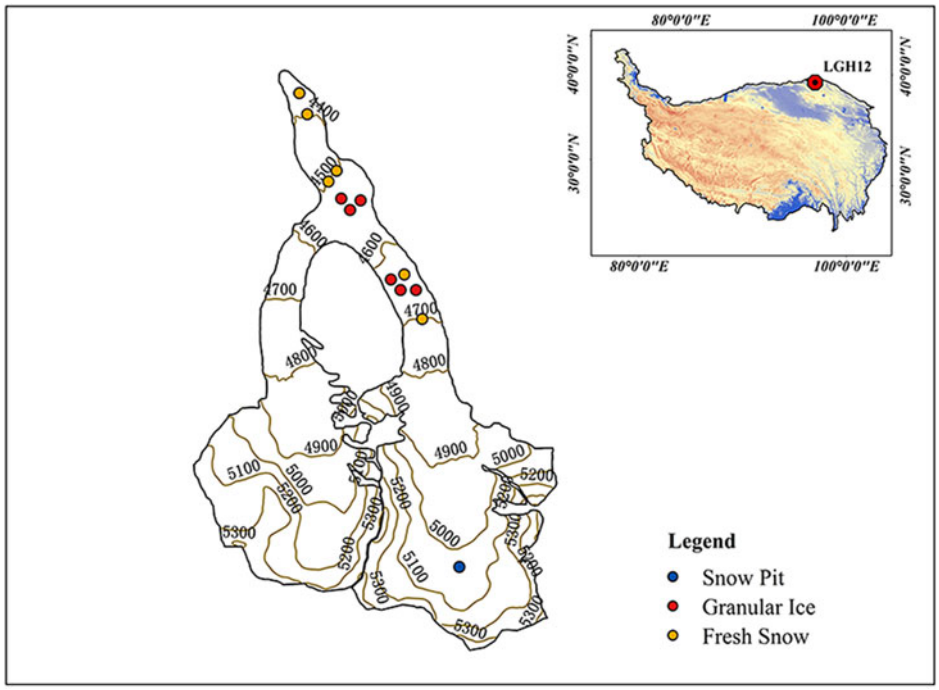

Fig. 1. Location of the LHG and the sampling sites in this glacier.

north (Xu and others, 2013). Like other glaciers on the TP, LHG has been experiencing significant and accelerating thinning and shrinkage since the mid-1990s (Du and others, 2008; Zhang and others, 2012). The average snow line of LHG retreated from 4800 to 4900 m between 1959 and 2006 (Du and others, 2008), and remote-sensing imagery shows the snow line at ~5000 m in recent years.

Six surface fresh snow and six surface granular ice samples were collected on 23 September 2015 in the ablation zone using a stainless steel scoop (Table 1). Granular ice samples represent aged snow that is subject to melting–freezing cycles. All samples were collected in a precleaned glass bottle (soaked in 1% alconox solution overnight, rinsed with Milli-Q water, and combusted at 400 °C for 6 h). In addition, a snow pit was dug in the accumulation zone at 5050 m a.s.l. on LHG on 25 August 2015 (Yan and others, 2016). Snow samples were collected in Whirl-Pak bags (Whirl-Pak®, Nasco, USA) using a Teflon ice scoop continuously at 5 cm depth intervals from the bottom to the top of the snow pit by personnel wearing clean suits, masks and gloves. In total, 23 snow samples were collected from the pit. The samples were all stored in the dark using a cooler box during 1–2 days of transport. After arriving at the laboratory, they were stored at −18 °C until analysis. Prior to analysis, they were melted at room temperature in a dark environment. Once completely melted, they were filtered through a 0.45 μm capsule filter (Pall AquaPrep 600) using a precleaned filter holder.

DOC analysis

Filtered fresh snow and granular ice samples were first analyzed for DOC. In order to remove inorganic carbonates, 100 μL of 10% hydrochloric acid was used to acidify a 10 mL aliquot of melted fresh snow and granular ice sample. The sample was then analyzed using a Vario EL CN analyzer (Elementar, Hanau, Germany). The oxidization of non-purgable organic carbon in the sample at a combusting temperature of 850 °C in a carrier gas with controlled O_2 concentration made gases containing carbon converted to CO_2, which was measured using a non-dispersive infrared analyzer (Xu and others, 2015).

We adopted the DOC concentration data for snow pit samples from LHG that were presented by Yan and others (2016). Their study focused on the bioavailability and light-absorbing features of DOC. In this case, the DOC concentrations of snow pit samples were analyzed by using a TOC-5000A analyzer (Shimadzu Corp, Kyoto, Japan). Acidified water samples (10 mL) were placed in muffled glass vials and sparged immediately before analysis. Sparged samples (100 μL) were injected into a combustion

Table 1. Sampling information for snow, ice and snow pit in this study

Sample type	Sampling date	Altitude m	Depth cm	Number (*n*)
Fresh snow 1	23 September 2015	4300–4500	Surface snow	3
Fresh snow 2	24 September 2015	4550–4650	Surface snow	3
Granular ice 1	21 September 2015	4500–4700	Surface ice	3
Granular ice 2	22 September 2015	4300–4500	Surface ice	3
Warm period snow 1	25 August 2015	5050	5–35	7
Warm period snow 2	25 August 2015	5050	40–45, 100–115	6
Cold period snow 1	25 August 2015	5050	50–70	5
Cold period snow 2	25 August 2015	5050	75–95	5

https://doi.org/10.1017/aog.2018.20 Published online by Cambridge University Press

tube (the oxygen carrier gas was passed through and the combustion tube was heated to 680 °C) containing a Shimadzu catalyst (0.5% Pt on alumina). After passing through the combustion tube, the gas stream was bubbled through a 25% H_3PO_4 solution and passed through an electronic dehumidifier and halogen scrubber before entering the detector. The non-dispersive infrared detector and the integrator in the Shimadzu instrument were used without modification to quantify CO_2.

These two different DOC analyzers employ a similar analytical method. The only difference being that the Vario EL CN analyzer can reach a higher combusting temperature (860 °C) than the TOC-5000A analyzer (680 °C), which led to a somewhat higher DOC concentration being determined by the former.

Absorption measurements

Measurements of light absorbance of all samples were analyzed using an ultraviolet-visible (UV-Vis) absorption spectrophotometer (UV-2700, Shimadzu, Japan) with a 5 cm quartz cuvette. The spectrum ranged from 200 to 900 nm with 1 nm step. The measurement used Milli-Q water sample as reference whose mean absorbance at 690–700 nm was subtracted for baseline correction of each absorbance spectrum. Optical density (absorbance value) and the corresponding absorption coefficient were obtained from

$$a(\lambda) = 2.303 \times A(\lambda)/L \quad (1)$$

where $A(\lambda)$ is the measured absorbance for wavelength λ, L is the path length of the optical cell ($L = 0.05$ m) and the factor 2.303 is common-to-natural logarithm transformation.

Isotope analysis

All the isotope data of snow pit samples were analyzed using a Picarro-2130i liquid water isotope analyzer (Picarro Inc., Santa Clara, CA) with an analytical precision of ±0.1‰ for $\delta^{18}O$, and ±0.4‰ for δD. The oxygen isotopic ratio ($\delta^{18}O$) was then used as an air temperature index (Tian and others, 2001; Cui and others, 2014) (Fig. 2), such that snow samples in the snow pit were classified into warm or cold periods using a threshold $\delta^{18}O$ value of −14. 13 samples were grouped into the warm period and 10 samples were grouped into the cold period.

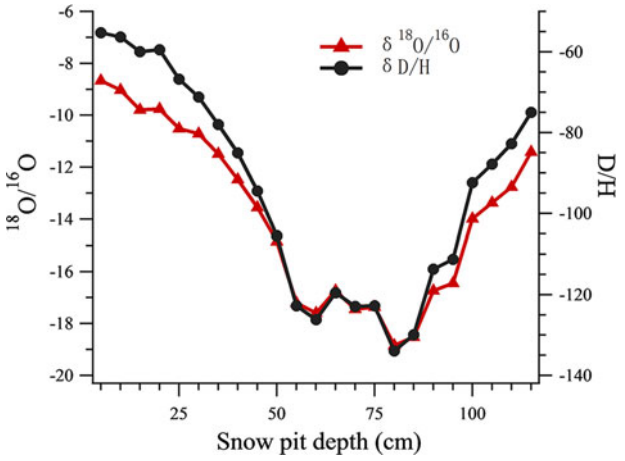

Fig. 2. The $\delta^{18}O$ record and δD record at different depths of the snow pit.

Three-dimensional fluorescence measurement

The excitation–emission matrix (EEM) fluorescence of samples was determined using a Hitachi F-7000 fluorescence spectrometer (Hitachi High-Technologies, Tokyo, Japan) equipped with a 150 W xenon arc lamp as the light source. Fluorescence scans were performed at 5 nm intervals from 250 to 450 nm excitation and monitored at 1 nm intervals from 250 to 600 nm emission. The spectra were recorded at a scan rate of 2400 nm min^{-1} using excitation and emission slit bandwidths of 5 nm.

All scans were Raman-corrected by subtracting the spectrum for Milli-Q water scanned under identical conditions. Rayleigh scatter effects were eliminated by replacing the EEM triangular regions of emission wavelength (wavelengths ⩽ excitation wavelength + 15 nm), and (wavelengths ⩾2 × excitation wavelength − 20 nm), with zeros (Zhang and others, 2010; Zhou and others, 2015). The EEMs were corrected for inner filter effects with absorption spectra obtained on a Shimadzu UV-2700 spectrophotometer with a 5 cm quartz cuvette and with Milli-Q water as a reference (Zhou and others, 2015). The fluorescence was finally calibrated to the water Raman signal at an excitation wavelength of 350 nm (Lawaetz and Stedmon, 2009), and the fluorescent results are given in Raman units (RUs). Excitation wavelengths at 200–225 nm and emission wavelengths at 250–299 and 550–600 nm were deleted in order to further eliminate unreliable instrumental measurements in these regions.

Parallel factor analysis (PARAFAC) modeling

PARAFAC, a three-way method, is applied to divide the CDOM fluorescence into separate fluorescent signals (Stedmon and Bro, 2008). This analysis was carried out with MATLAB 2015b software using the DOMFluor toolbox. PARAFAC was applied to our EEM dataset (35 samples × 250 emissions × 45 excitations), with some analytical and statistical assumptions as reported by Stedmon and Bro (2008).

The characteristic parameters of EEM fluorescence spectroscopy, such as biological index (BIX) and humification index (HIX), were critical in determining the DOM sources (Fellman and others, 2010). The BIX, which measures the proportion of biogenic and exogenous organic matter, is the ratio of emission intensity at 380 nm divided by the emission intensity maximum observed between 420 and 435 nm, obtained at excitation 310 nm (Parlanti and others, 2000; Fellman and others, 2010). Values of BIX < 0.6 show fewer authigenic components, while BIX ranging from 0.8 to 1.0 indicates that biological or microbial origin mainly contributes to DOM (Birdwell and Engel, 2010). The HIX demonstrates the humification or degree of maturity of organic matter. HIX is obtained from the ratio of the fluorescence peak value within emission wavelength 435–480 and 300–345 nm, at the excitation wavelength 254 nm (Ohno, 2002).

Electrospray ionization (ESI)-Fourier transform ion cyclotron resonance mass spectrometry (FT-ICR MS) analysis

Prior to ESI-FT-ICR MS analysis, the samples were preconcentrated using PPL (Agilent Bond Elut-PPL cartridges, 500

https://doi.org/10.1017/aog.2018.20 Published online by Cambridge University Press

mg, 6 mL) solid phase extraction (SPE) cartridges and followed a protocol that has already been described (Dittmar and others, 2008; Feng and others, 2016). Generally, three column volumes of acidified ultrapure water (pH = 2, LC-MS grade HCl) and 20 mL LC-MS grade methanol were used to prime the PPL cartridges. Using 0.1 M LC-MS grade HCl, ~150 mL of each sample was brought to pH = 2, and then passed through the PPL cartridges at 1 mL min^{-1}. When the cartridges were dried, ~10 mL of methanol was applied to elute all samples, which were then concentrated to ~1 mL using N_2 and promptly stored at 4 °C. Following the same manner, Milli-Q water was processed as a procedural blank.

The samples were analyzed using a solariX XR FT-ICR MS (Bruker Daltonik GmbH of Bremen, Germany) equipped with a 9.4 T superconducting magnet (Bruker Biospin, Wissembourg, France) and the Paracell analyzer cell. The samples were ionized in positive ion modes using the ESI ion source (Bruker Daltonik GmbH, Bremen, Germany). Ions were accumulated in a hexapole ion trap for 1.0 s before being transferred to the ICR cell. Data of 4 M word size were recorded to acquire the time-domain signal. The detection mass spectrum ranged from *m/z* 150 to *m/z* 800. The signal-to-noise ratio (S/N) and dynamic range were strengthened according to 100 continuous FI-ICR transients. Procedural blanks were also obtained in accordance with the same procedure to check potential contamination. A typical mass-resolving power ($m/\Delta m$ 50%, in which Δm 50% is the magnitude of the mass spectral peak full width at half-maximum peak height) was calculated to be over 400 000 at *m/z*, with the absolute mass error <0.5 ppm. It is important to note that the mass spectra of different characteristic molecules may be affected by different SPE, ionization mechanism, parameters and data acquisitions. For using PPL SPE cartridge, the most hydrophilic compounds such as inorganic ions, and low-molecular-weight organic molecules such as organic acids and sugars were removed, whereas the relatively hydrophobic fraction was retained.

Molecular formula assignment

Molecular formula assignments for all ions were acquired based on a S/N of mass peak >10 with a mass tolerance of ±1.5 ppm using a customized software. Molecular formulae with the maximum number of atoms were set to: 30 ^{12}C, 60 ^{1}H, 20 ^{16}O, 3 ^{14}N, 1 ^{32}S, 1 ^{13}C, 1 ^{18}O and 1 ^{34}S. Identified formulas containing isotopomers (i.e. ^{13}C, ^{18}O or ^{34}S) were not considered. Double bond equivalence (DBE) = $(2c + 2 - h + n)/2$ was adopted to calculate the number of double bonds and rings in regard to the chemical formula $C_cH_hO_oN_nS_S$ (McLafferty and Turecek, 1993). The van Krevelen diagram was then employed as a graphical method for qualitatively analyzing the major classes of compounds (such as lipids, aliphatic/proteins, carbohydrates, etc.) within the complicated spectrum. This diagram represents an element–ratio plot, in which each point represents the molar ratio of hydrogen to carbon (H/C) on the *y*-axis and molar ratio of oxygen to carbon (O/C) on the *x*-axis for a specific molecule (Grannas and others, 2006; Hockaday and others, 2009; Ide and others, 2017). We also combined the modified aromaticity index (AI_{mod}) (Koch and Dittmar, 2006, 2016) to identify the biomolecular class. AI_{mod} is a measure of the probable aromaticity for a given molecular formula assuming that half of the oxygen atoms are doubly bound and half are present as σ bonds and was calculated as:

$$AI_{mod} = \frac{(1 + C - 0.5O - S - 0.5[N + P + H])}{(C - 0.5O - N - S - P)} \quad (2)$$

Formulas with $AI_{mod} \geqslant 0.5$ and <0.67 were assigned as aromatics, while formulas with $AI_{mod} \geqslant 0.67$ were assigned as condensed aromatics (Koch and Dittmar, 2006). Seven biomolecular classes in the molecular compound were partitioned on account of the values of O/C and H/C (Hockaday and others, 2009; Antony and others, 2014; Lu and others, 2015). The seven classes were (1) lipids ($0 \leqslant O/C < 0.3$, $1.5 < H/C < 2.4$), (2) aliphatic/proteins ($0.3 \leqslant O/C \leqslant 0.67$, $1.5 < H/C < 2.4$), (3) carbohydrates/amino sugars ($0.67 < O/C < 1.2$, $1.5 < H/C < 2.4$), (4) unsaturated hydrocarbons ($0 < O/C < 0.1$, $0.7 \leqslant H/C \leqslant 1.5$), (5) lignins/carboxyl-rich alicyclic acids ($0.1 \leqslant O/C \leqslant 0.67$, $0.7 \leqslant H/C \leqslant 1.5$, $AI < 0.67$), (6) tannins ($0.67 < O/C < 1.2$, $0.5 \leqslant H/C \leqslant 1.5$, $AI < 0.67$) and (7) condensed aromatics ($0 < O/C \leqslant 0.67$, $0.2 \leqslant H/C < 0.7$, $AI \geqslant 0.67$).

RESULTS AND DISCUSSION

DOC concentrations and UV-Vis properties of the DOM

DOC concentrations in the fresh snow ranged from 2.00 to 2.61 mg L^{-1} (Fig. 3a), which is comparable with the values reported from Mount Yulong (2.03 mg L^{-1}) (Niu and others, 2016) but higher than those from Dongkemadi Glacier on Mount Tanggula (0.32 mg L^{-1}) in the central TP, collected during summer 2015 (Feng and others, 2017). Granular ice samples had DOC concentrations ranging from 1.40 to 1.57 mg L^{-1}, lower than those of the fresh snow samples,

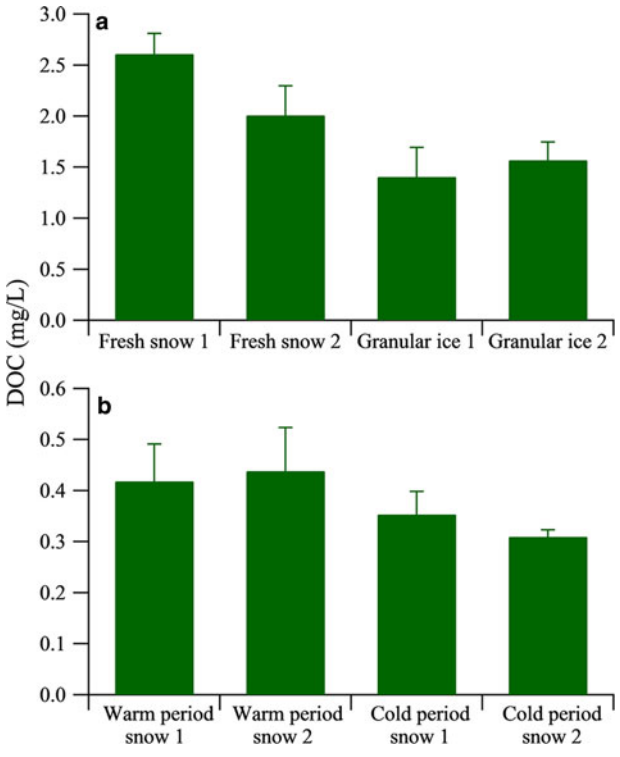

Fig. 3. Average mass concentrations of DOC in fresh snow, granular ice (a) and snow pit samples (b). The data of DOC concentration of snow pit samples are adopted from Yan and others (2016). The error bars indicate the Std dev. (1σ).

https://doi.org/10.1017/aog.2018.20 Published online by Cambridge University Press

likely due to photolysis of DOC and/or loss during the snow-melt–freezing process. DOC concentration in the snow pit samples had higher values during the warm period, ranging from 0.42 to 0.44 mg L^{-1}, and lower values during the cold period, ranging from 0.35 to 0.31 mg L^{-1} (Fig. 3b) (Yan and others, 2016). The occurrence of higher values during the warm period is due to the development of mountain-valley wind circulation from planetary boundary layer to free troposphere (Xu and others, 2013). In addition, the higher DOC concentration in the warm period could also be from microbial activity during the melting process as illustrated by our FT-ICR MS analysis below.

The average absorption coefficient of fresh snow samples and granular ice samples had higher values for short wavelengths and decreased sharply above 240 nm (Fig. 4a). The fresh snow showed stronger absorption characteristics within the range of 200–240 nm than that of the granular ice, suggesting that there were more chromophores in fresh snow samples. These chromophores could be double-bond olefin compounds (Zhao, 2012) and/or the amide group of the polypeptide backbone (Mundi, 2012). The absorption was lower in the snow pit samples than in the fresh snow and granular ice, consistent with their different DOC concentrations. The sum of absorption between 200 and 400 nm showed a significant correlation with DOC concentration in all snow category samples ($R^2 = 0.69$, $P < 0.05$). But the average absorption from snow samples deposited in the snow pit during the cold period and those deposited during the warm period did not differ markedly (Fig. 4b). In addition, absorption was weak for snow pit and granular ice samples within the range of 250–320 nm compared with fresh snow, indicating different chromophores.

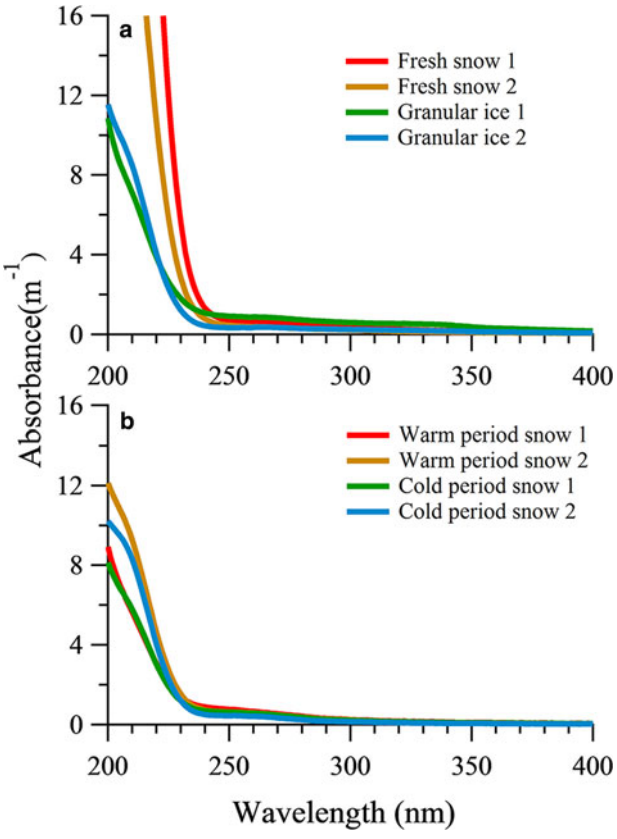

Fig. 4. UV-Vis absorbance spectra of DOM in fresh snow, granular ice samples (a) and snow pit samples (b).

Fluorescent components identified by EEM-PARAFAC and fluorescence indices of DOM

The fluorescence results from a total of 35 samples (comprising 23 snow pit samples, six fresh snow and six granular ice samples) were used to perform PARAFAC analysis, and four fluorescent components were identified with unique spectra in each component (Fig. 5). Table 2 summarizes the excitation and emission characteristics of each fluorescent component in our study and the characteristics of components defined by other studies. Two of the four components we identified can be described as humic-like, or derived from humic substances (components 1 and 4), whereas components 2 and 3 are protein-like. Component 1 (C1) had two excitation maxima at 240 and 305 nm and an emission maximum at 392 nm. The spectral features of C1 were similar to the humic-like components, which were likely associated with biological activity (Coble, 1996; Fellman and others, 2010). Murphy and others (2011) described a similar peak to microbial humic-like fluorescence in water samples from recycled-water treatment plants. Two excitation maxima at 270 and 345 nm and an emission maximum at 452 nm were observed for component 4 (C4), which represents older substances derived from terrestrial plant or soil organic matter (Coble and others, 1998; Fellman and others, 2010).

Component 2 (C2) showed two excitation maxima at <240 and 275 nm and an emission maximum at 340 nm, which closely resembles those of tryptophan-like fluorophores. Fellman and others (2010) found this spectrum could come from free amino acids or amino acids bound in protein molecular structure, which are intact proteins or less degraded peptide material. Typically, tryptophan is associated with autochthonous productions of DOM through biological degradation (Dubnick and others, 2010). Component 3 (C3) was found in the EEM region corresponding to protein-like fluorophores with excitation maximum at 265 nm and emission maximum at 316 nm. The spectral pattern of C3 resembles the tyrosine-like fluorophore and may indicate more degraded peptide material from autochthonous production of DOM (Fellman and others, 2010).

The two protein-like components (C2 and C3) accounted for more than 60% (range from 60.87 to 67.93% in all samples) of the modeled fluorescence, which suggests a significant microbial source of DOM in these samples (Table 3). This is consistent with many previous results showing that DOM in a glacier environment comes predominantly from microbial sources and has a high ratio of protein-like to humic-like components (Lafrenière and Sharp, 2004; Barker and others, 2009, 2013; Feng and others, 2016). The relative contribution of protein-like components (C2 and C3) in snow pit samples (64.41–67.93%) was higher than that of fresh snow and granular ice (60.87–65.86%), whereas the proportion of humic-like components (C1 and C4) was lower in the snow pit (32.06–35.59%) than in fresh snow and granular ice (34.49–39.13%). In addition, the snow samples during the cold period contained higher protein-like components (C2 and C3) (67.74–69.93%) and lower humic-like components (C1 and C4) (32.06–32.26%) compared with the snow samples during the warm period (64.41–67.58% for C2 and C3 and 32.42–35.59% for C1 and C4). Note that the relative contribution of protein-like components and humic-like components showed no significant difference between different samples likely due to the small number of samples.

https://doi.org/10.1017/aog.2018.20 Published online by Cambridge University Press

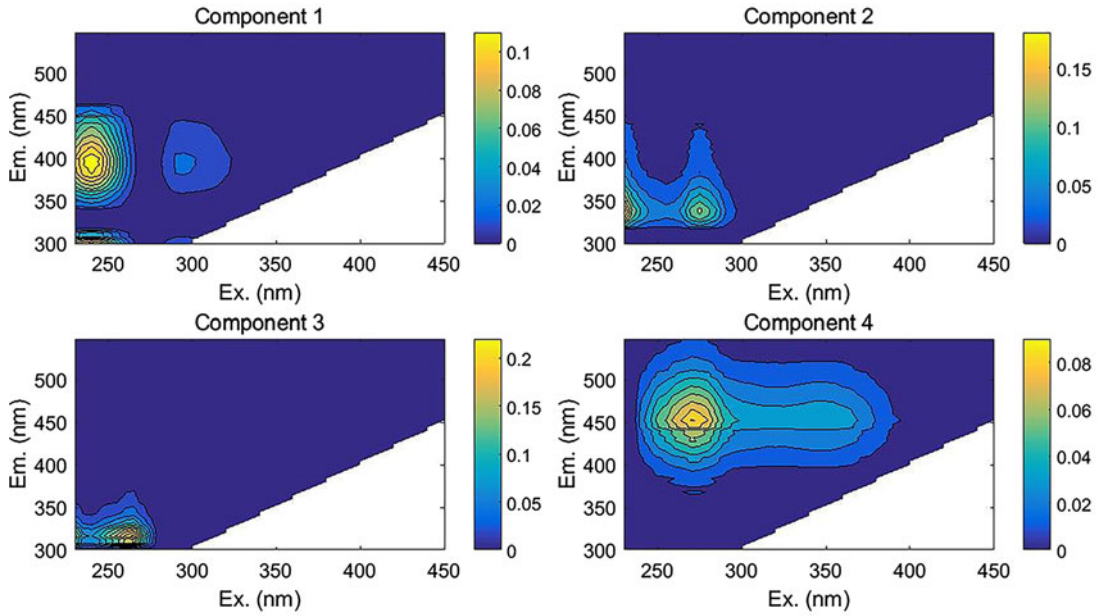

Fig. 5. EEMs for the four-component PARAFAC model.

The indexes BIX and HIX were proposed to assess the relative contribution of autochthonous DOM and humification of DOM in the natural aquatic environment (Huguet and others, 2009; Birdwell and Engel, 2010). The DOM in fresh snow, granular ice, and snow pit samples have low values of BIX (<1.0) and HIX (<1.2), which indicate a fresh DOM source derived predominantly from microbes (Birdwell and Engel, 2010).

BIX values were lower, whereas HIX values were higher, in fresh snow than in granular ice. These results suggest that DOM in granular ice contained a higher fraction from autochthonous than fresh snow, and that fresh snow contained more humic material which was likely from the ambient aerosol (Voisin and others, 2012). BIX and HIX values in snow pit samples showed a similar situation to granular ice, with higher BIX values (0.81–0.90) and lower HIX values (0.54–0.61) (Table 3). Specifically, the snow samples during the cold period showed higher BIX values and lower HIX values compared with the warm period, which suggest relatively higher contribution of autochthonous DOM in the samples during the cold period and higher humification DOM in the samples during the warm period.

Molecular composition of DOM from ultra-high-resolution FT-ICR MS

The van Krevelen diagram shows that all samples were dominated by lipid- and aliphatic/protein-type components (Fig. 6), which account for more than 70% of the assigned peaks (Table 4). This phenomenon is similar to those found in surface snow samples from the East Antarctic ice sheet and the cryoconites in LHG (Antony and others, 2014; Feng and others, 2016). Previous studies have suggested that the predominant lipid- and aliphatic/protein-like components were produced by a diverse assemblage of bacteria, archaea and eukarya which could degrade and produce DOM in the Antarctic snowpack (Antony and others, 2016, 2017). In addition to the predominantly autochthonous microbial material, terrestrial components were also found in each type of sample, as shown by the presence of tannin and lignin/CRAM molecules (12.4–20.6%) in the van Krevelen diagrams (Fig. 6). These components could be supplied by long-range atmospheric transport of terrestrial organic matter (Li and others, 2016) and local surrounding debris. It is interesting to note that the fresh snow samples have a similar composition to other samples, i.e. more microbially derived DOM, suggesting that the aerosols in this

Table 2. The four components identified by the PARAFAC model, with maximum excitation/emission wavelengths and description (Coble, 1996; Coble and others, 1998; And and Mcknight, 2005; Fellman and others, 2010)

Component	Excitation maxima nm	Emission maxima nm	Fluorophore type	Description
C1	240, 305	392	Humic-like	Low molecular weight, common in marine environments associated with biological activity but can be found in wastewater, wetland and agricultural environment
C2	<240, 275	340	Protein-like (tryptophan-like)	Amino acids, free or bound in proteins, fluorescence resembles free tryptophan, may indicate intact proteins or less degraded peptide material
C3	265	316	Protein-like (tyrosine-like)	Amino acids, free or bound in proteins, fluorescence resembles free tyrosine, may indicate more degraded peptide material
C4	270, 345	452	Humic-like	UVC humic-like: high molecular weight (and aromatic) humic, widespread

https://doi.org/10.1017/aog.2018.20 Published online by Cambridge University Press

Table 3. HIX and BIX for DOM extracted from the samples in this study, and the average relative contributions of the four components identified by the PARAFAC model

Sample type	BIX	HIX	% C1	% C2	% C3	% C4	% C2 + C3	% C1 + C4
Fresh snow 1	0.46	1.18	32.44	33.25	27.62	6.69	60.87	39.13
Fresh snow 2	0.61	0.98	26.99	31.40	34.01	7.50	65.41	34.49
Granular ice 1	0.81	0.54	27.81	33.39	28.98	9.81	62.37	37.62
Granular ice 2	0.90	0.61	25.06	32.71	33.15	9.07	65.86	34.13
Warm period snow 1	0.90	0.45	24.67	32.97	34.61	7.75	67.58	32.42
Warm period snow 1	0.84	0.40	28.18	32.30	32.11	7.41	64.41	35.59
Cold period snow 1	0.96	0.41	25.08	31.18	36.75	6.98	67.93	32.06
Cold period snow 2	0.94	0.36	24.05	37.31	30.43	8.21	67.74	32.26

remote area of the TP mostly originated from natural sources. Primary biological aerosol particles (PBAPs) including bacteria, spores and pollen, could be more abundant during summer due to more favorable air temperature and humidity conditions (Toprak and Schnaiter, 2013), which could be the source of the microbially derived components (including lipids and aliphatic/proteins) in fresh snow.

The van Krevelen plots were also classified by the molecular class, i.e. CHO, CHN and CHON (Fig. 6). The contributions of these classes for each category sample are shown in Table 5. CHO-only molecules dominated the compounds (69.7–78.3%), followed by CHON compounds (21–29.7%) and CHN-only molecules (0.3–0.9%). We performed an intercomparison of DOM components in different category samples and found slight differences in some assigned compounds. DOM in fresh snow and granular ice contained fewer lipid- and protein-type components and more lignin- and tannin-type components than the snow pit (Table 4). N-containing molecules (CHN and CHON) were also fewer in fresh snow and granular ice than in the snow pit (Table 5), implying that DOM in fresh snow and granular ice was more affected by terrestrial sources, while DOM in the snow pit was mainly affected by microbial activity in situ. The higher DBE values in fresh snow and granular ice samples than in snow pit samples (Table 5) also suggest that allochthonous sources such as terrestrial materials (Lawson and others, 2014) may be the major contributor of DOM in fresh snow and granular ice.

Snow samples during the warm period had more terrestrially derived DOM (lignin- and tannin-type components) but less microbially derived originated DOM (lipid- and aliphatic/protein-type components) than the cold period (Table 4), which was consistent with results from the EEMs. This may result from more precipitation events occurring during the warm season in this region, so that more terrestrial-originated DOM could be transported and deposited with snowfall. The proportion of lipid- and aliphatic/protein-type components was lower in fresh snow than in granular ice, while that of lignin- and tannin-type components was higher than in granular ice (Table 4). The proportion of lipid- and aliphatic/protein-type components did not vary significantly between fresh snow and granular ice likely due to the small number of samples, yet they still showed obvious changes during the melting–freezing process (from fresh snow to granular ice). This trend was consistent with the variation of HIX, which showed a significant correlation between them (Table 3) ($R^2 = 0.55$, $P < 0.05$). N-containing molecules (CHN and CHON) in fresh snow were fewer than in granular ice (Table 5). These results again suggest that fresh snow contained more terrestrial sources of DOM, and granular ice contained more DOM of microbial origin.

We also analyzed the effects of snowmelting on DOM compositions by directly comparing the unique and overlapping assigned molecular compounds in the fresh snow and granular ice samples using a simple Venn diagram (Fig. 7).

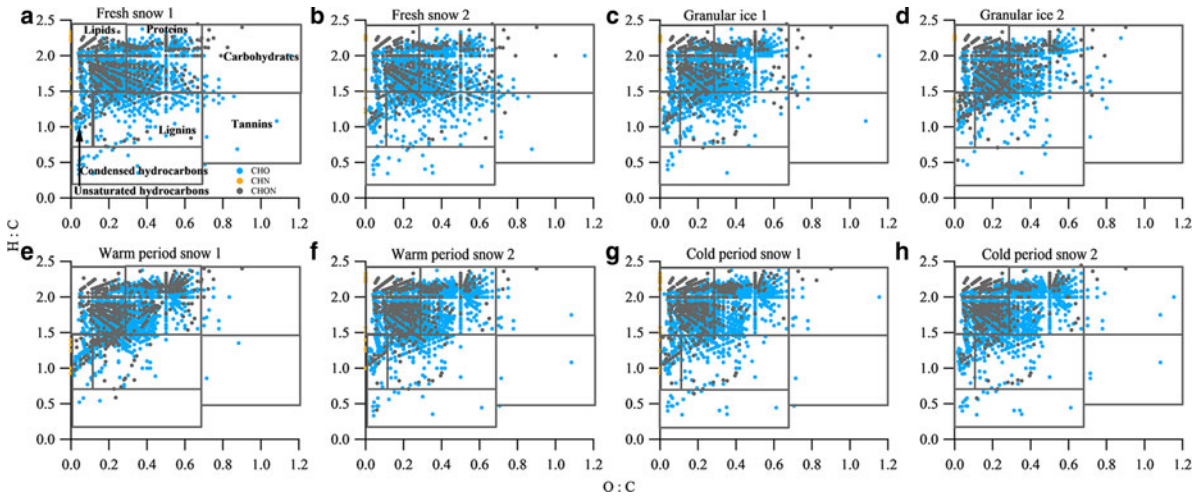

Fig. 6. van Krevelen diagrams for the mass spectra of samples of (a) fresh snow 1, (b) fresh snow 2, (c) granular ice 1, (d) granular ice 2, (e) warm period snow 1, (f) warm period snow 2, (g) cold period snow 1 and (h) cold period snow 2. The black lines in the van Krevelen diagram correspond to major classes of compounds that can be expected in DOM.

https://doi.org/10.1017/aog.2018.20 Published online by Cambridge University Press

Table 4. The number of molecular formulas identified, and % of molecular formulas assigned to each defined compound class as revealed by FT-ICR MS for DOM samples isolated from the fresh snow, granular ice and snow pit samples in LHG

Sample type	Formulas assigned	Lipids and aliphatic/ proteins (%)	Carbohydrates (%)	Unsaturated hydrocarbons (%)	Lignins and tannins (%)	Condensed aromatics (%)
Fresh snow 1	1706	1293 (75.97%)	23 (1.3%)	59 (3.5%)	313 (18.3%)	17 (1%)
Fresh snow 2	1619	1183 (73.1%)	18 (1.1%)	68 (4.2%)	333 (20.6%)	17 (1%)
Granular ice 1	1613	1215 (75.4%)	16 (1%)	74 (4.6%)	299 (18.5%)	8 (0.5%)
Granular ice 2	1349	1016 (75.3%)	15 (1.1%)	78 (5.8%)	234 (17.4%)	6 (0.4%)
Warm period snow 1	1849	1438 (77.8%)	24 (1.3%)	76 (4.1%)	307 (16.6%)	4 (0.2%)
Warm period snow 2	1866	1434 (80.1%)	17 (0.9%)	71 (3.8%)	269 (14.4%)	14 (0.8%)
Cold period snow 1	1712	1388 (81.1%)	16 (1%)	76 (4.4%)	212 (12.4%)	18 (1.1%)
Cold period snow 1	1701	1383 (81.3%)	16 (1%)	69 (4.1%)	215 (12.6%)	18 (1%)

Table 5. The average molecular weight, the average of DBE, and the number and % containing of CHO, CHON, CHN classes as revealed by FT-ICR MS for DOM samples isolated from the fresh snow, granular ice and snow pit samples in LHG

Sample type	Mean molecular weight	DBE	CHO (%)	CHON (%)	CHN (%)
Fresh snow 1	365	4.14	1311 (76.8%)	381 (22.4%)	14 (0.8%)
Fresh snow 2	367	4.37	1268 (78.3%)	340 (21%)	11 (0.7%)
Granular ice 1	393	4.45	1242 (77%)	360 (22.3%)	11 (0.7%)
Granular ice 2	395	4.83	940 (69.7%)	401 (29.7%)	8 (0.6%)
Warm period snow 1	420	4.51	1349 (72.9%)	495 (26.8%)	5 (0.3%)
Warm period snow 2	379	3.86	1393 (74.7%)	460 (24.6%)	13 (0.7%)
Cold period snow 1	387	3.89	1250 (73%)	446 (26.1%)	16 (0.9%)
Cold period snow 2	379	3.81	1287 (75.7%)	402 (23.6%)	12 (0.7%)

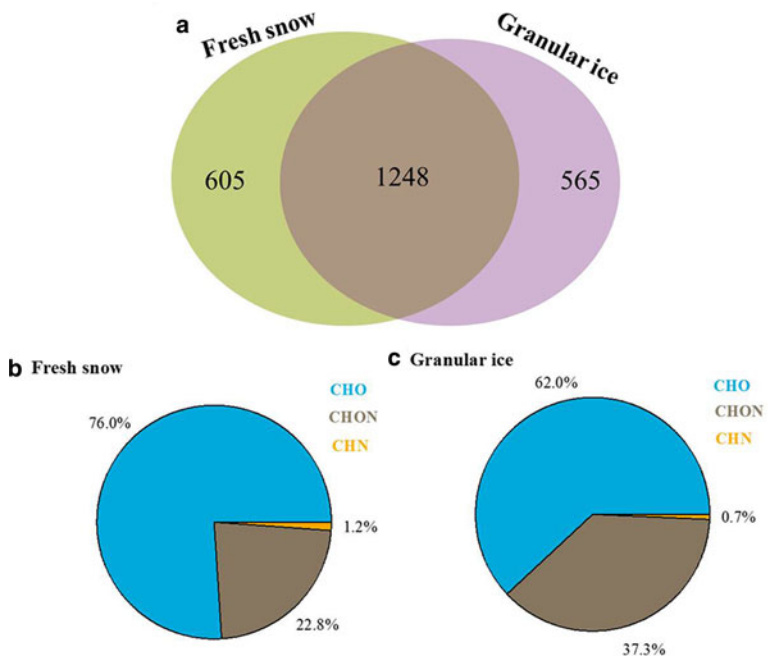

Fig. 7. (a) Two-way Venn diagram for molecular formulas between fresh snow and granular ice. The numbers in the diagram are the percentage of the common and unique formulas to each type of sample. (b) and (c) Mean contributions of different molecules identified from the FT-ICR mass spectra for the unique components in fresh snow and granular ice.

About 40% (1248) of the identified molecular components overlapped, indicating that DOM in fresh snow and DOM in granular ice have a high degree of similarity. However, the unique molecular components in granular ice (565, accounting for 23.4% of total assigned molecules) contain more CHON molecules (37.3%) and suggest a higher bioavailability than those in fresh snow (22.8%), suggesting microbial modification of DOM during the snowmelting process.

https://doi.org/10.1017/aog.2018.20 Published online by Cambridge University Press

CONCLUSIONS

Our study has presented the DOC concentration, UV-Vis properties, fluorescent components and molecular information of the DOM in different samples and seasons in LHG. In summary, the DOC concentration showed higher values in fresh snow and snow samples during the warm period compared respectively with granular ice and snow samples during the cold period. The UV-Vis properties of all types of samples followed the same pattern as DOC concentration. EEMs combined with PARAFAC identified four fluorescent components of DOM in all samples, two protein-like components (C2 and C3), one microbial humic-like component (C1) and one humic-like component (C4), indicating an obvious microbial origin of DOM in this glacier. Based on the ESI-FT-ICR-MS results, DOM in fresh snow and granular ice contained less microbially derived DOM (lipid- and protein-type components) and more terrestrially derived DOM (lignin- and tannin-type components) than that in the snow pit samples. Here, snow deposited during the warm period had more terrestrial DOM but less microbial DOM when compared with snow deposited during the cold period. This suggests that there was more bioavailable DOM in the older snow that has been stored on the glacier. More interestingly, the unique DOM components in granular ice (aged snow on the glacier) contain more CHON molecules than fresh snow, indicating that melt–refreeze and other processes could modify the DOM composition and enhance the bioavailability of DOM over time.

ACKNOWLEDGEMENTS

This research was supported by grants from the National Natural Science Foundation of China (41771079 and 41421061), the Key Laboratory of Cryospheric Sciences Scientific Research Foundation (SKLCS-ZZ-2017-01) and the Chinese Academy of Sciences Hundred Talents Program. We thank the colleagues for continuing support and discussion.

REFERENCES

And RMC and Mcknight DM (2005) Fluorescence spectroscopy reveals ubiquitous presence of oxidized and reduced quinones in dissolved organic matter. *Environ. Sci. Technol.*, **39**(21), 8142–8149

Antony R and 5 others (2014) Origin and sources of dissolved organic matter in snow on the east Antarctic ice sheet. *Environ. Sci. Technol.*, **48**(11), 6151–6159

Antony R and 5 others (2016) Microbial communities associated with Antarctic snow pack and their biogeochemical implications. *Microbiol. Res.*, **192**, 192–202

Antony R and 7 others (2017) Molecular insights on dissolved organic matter transformation by supraglacial microbial communities. *Environ. Sci. Technol.*, **51**(8), 4328–4337

Barker JD, Sharp MJ and Turner RJ (2009) Using synchronous fluorescence spectroscopy and principal components analysis to monitor dissolved organic matter dynamics in a glacier system. *Hydrol. Processes*, **23**(10), 1487–1500

Barker JD, Dubnick A, Lyons WB and Chin YP (2013) Changes in dissolved organic matter (DOM) fluorescence in proglacial Antarctic streams. *Arct. Antarct. Alp. Res.*, **45**(3), 305–317

Birdwell JE and Engel AS (2010) Characterization of dissolved organic matter in cave and spring waters using UV-Vis absorbance and fluorescence spectroscopy. *Org. Geochem.*, **41**(3), 270–280

Coble PG (1996) Characterization of marine and terrestrial DOM in seawater using excitation-emission matrix spectroscopy. *Mar. Chem.*, **51**(4), 325–346

Coble PG, Del Castillo CE and Avril B (1998) Distribution and optical properties of CDOM in the Arabian Sea during the 1995 southwest monsoon. *Deep Sea Res., Part II*, **45**(10–11), 2195–2223

Cui X and 6 others (2014) Chemical characteristics and environmental records of a snow-pit at the glacier no. 12 in the Laohugou Valley, Qilian Mountains. *J. Earth Sci.*, **25**(2), 379–385

Dittmar T, Koch B, Hertkorn N and Kattner G (2008) A simple and efficient method for the solid-phase extraction of dissolved organic matter (SPE-DOM) from seawater. *Limnol. Oceanogr.: Methods*, **6**(6), 230–235

Du W, Qin X and Liu Y (2008) Variation of the Laohugou glacier no. 12 in the Qilian Mountains. *Journal of Glaciology & Geocryology*, **30**(3), 373–379

Dubnick A and 7 others (2010) Characterization of dissolved organic matter (DOM) from glacial environments using total fluorescence spectroscopy and parallel factor analysis. *Ann. Glaciol.*, **51**(56), 111–122

Fellman JB, Hood E and Spencer RGM (2010) Fluorescence spectroscopy opens new windows into dissolved organic matter dynamics in freshwater ecosystems: a review. *Limnol. Oceanogr.*, **55**(6), 2452–2462

Feng L and 6 others (2016) Chemical composition of microbe-derived dissolved organic matter in Cryoconite in Tibetan plateau glaciers: insights from Fourier transform ion cyclotron resonance mass spectrometry analysis. *Environ. Sci. Technol.*, **50**(24), 13215–13223

Feng L and 8 others (2017) Physical and chemical evolution of dissolved organic matter across the ablation season on a glacier in the central Tibetan Plateau. *Biogeosci. Discuss.*, https://doi.org/10.5194/bg-2017-507

Grannas AM, Hockaday WC, Hatcher PG, Thompson LG and Ellen MT (2006) New revelations on the nature of organic matter in ice cores. *J. Geophys. Res.: Atmos.*, **111**(D4), 613–666

Guo W and 9 others (2015) The second Chinese glacier inventory: data, methods and results. *J. Glaciol.*, **61**(226), 357–372

Hockaday WC, Purcell JM, Marshall AG, Baldock JA and Hatcher PG (2009) Electrospray and photoionization mass spectrometry for the characterization of organic matter in natural waters: a qualitative assessment. *Limnol. Oceanogr.: Methods*, **7**(1), 81–95

Hood E, Battin TJ, Fellman J, O'Neel S and Spencer RGM (2015) Storage and release of organic carbon from glaciers and ice sheets. *Nat. Geosci.*, **8**(2), 91–96

Huguet A and 5 others (2009) Properties of fluorescent dissolved organic matter in the Gironde Estuary. *Org. Geochem.*, **40**(6), 706–719

Huss M (2011) Present and future contribution of glacier storage change to runoff from macroscale drainage basins in Europe. *Water Resour. Res.*, **47**(7), W07511

Ide J and 9 others (2017) Spatial variations in the molecular diversity of dissolved organic matter in water moving through a boreal forest in eastern Finland. *Sci. Rep.*, **7**, 42102

Koch B and Dittmar T (2006) From mass to structure: an aromaticity index for high-resolution mass data of natural organic matter. *Rapid Commun. Mass Spectrom.*, **20**(5), 926–932

Koch B and Dittmar T (2016) From mass to structure: an aromaticity index for high-resolution mass data of natural organic matter. *Rapid Commun. Mass Spectrom.*, **30**(1), 250–250

Lafrenière MJ and Sharp MJ (2004) The concentration and fluorescence of dissolved organic carbon (DOC) in glacial and nonglacial catchments: interpreting hydrological flow routing and DOC sources. *Arct. Antarct. Alp. Res.*, **36**(2), 156–165

Lawaetz AJ and Stedmon CA (2009) Fluorescence intensity calibration using the Raman scatter peak of water. *Appl. Spectrosc.*, **63**(8), 936

Lawson EC, Bhatia MP, Wadham JL and Kujawinski EB (2014) Continuous summer export of nitrogen-rich organic matter from

https://doi.org/10.1017/aog.2018.20 Published online by Cambridge University Press

the Greenland Ice Sheet inferred by ultrahigh resolution mass spectrometry. *Environ. Sci. Technol.*, **48**(24), 14248–14257

Li J, Qin X, Sun W, Zhang M and Yang J (2012) Analysis on micrometeorological characteristics in the surface layer of Laohugou no. 12 in Qilian Mountains. *Plateau Meteorol.*, **31**(2), 370–379

Li Q and 6 others (2016) Composition and sources of polycyclic aromatic hydrocarbons in cryoconites of the Tibetan Plateau glaciers. *Sci. Total Environ.*, **574**, 991

Liu Y, Xu J, Kang S, Li X and Li Y (2016) Storage of dissolved organic carbon in Chinese glaciers. *J. Glaciol.*, **1**(232), 1–5

Lu Y and 6 others (2015) Use of ESI-FTICR-MS to characterize dissolved organic matter in headwater streams draining forest-dominated and pasture-dominated watersheds. *PLoS One*, **10**(12), e0145639

McLafferty FW and Turecek F (1993) Interpretation of mass spectra. University Science Books, Sausalito, CA

Milner AM and 9 others (2017) Glacier shrinkage driving global changes in downstream systems. Proc. Natl. Acad. Sci. USA, **114**(37), 9770–9778

Mundi S (2012). Structural and functional characterization of red kidneybean (*Phaseolus vulgaris*) proteins and enzymatic protein-hydrolysates. University of Manitoba, Canada

Murphy KR and 6 others (2011) Organic matter fluorescence in municipal water recycling schemes: toward a unified PARAFAC model. *Environ. Sci. Technol.*, **45**(7), 2909–2916

Niu H and 5 others (2016) Chemical compositions of snow from Mt. Yulong, southeastern Tibetan Plateau. *J. Earth Syst. Sci.*, **125**(2), 1–14

Ohno T (2002) Fluorescence inner-filtering correction for determining the humification index of dissolved organic matter. *Environ. Sci. Technol.*, **36**(19), 742–746

Parlanti E, Wörz K, Geoffroy L and Lamotte M (2000) Dissolved organic matter fluorescence spectroscopy as a tool to estimate biological activity in a coastal zone submitted to anthropogenic inputs. *Org. Geochem.*, **31**(12), 1765–1781

Spencer RGM and 6 others (2014) Source and biolability of ancient dissolved organic matter in glacier and lake ecosystems on the Tibetan Plateau. *Geochim. Cosmochim. Acta*, **142**(1), 64–74

Stedmon CA and Bro R (2008) Characterizing dissolved organic matter fluorescence with parallel factor analysis: a tutorial. *Limnol. Oceanogr.: Methods*, **6**(11), 572–579

Stocker T and 9 others (2013) *IPCC, 2013: climate change 2013: the physical science basis. Contribution of working group I to the fifth assessment report of the intergovernmental panel on climate change*. Cambridge Univ. Press, Cambridge, UK, and New York, 1535 pp

Tian L, Masson-Delmotte V, Stievenard M, Yao T and Jouzel J (2001) Tibetan plateau summer monsoon northward extent revealed by measurements of water stable isotopes. *J. Geophys. Res.: Atmos.*, **106**(D22), 28081–28088

Toprak E and Schnaiter M (2013) Fluorescent biological aerosol particles measured with the Waveband Integrated Bioaerosol Sensor WIBS-4: laboratory tests combined with a one year field study. *Atmos. Chem. Phys.*, **13**(1), 225

Voisin D and 9 others (2012) Carbonaceous species and humic like substances (HULIS) in Arctic snowpack during OASIS field campaign in barrow. *J. Geophys. Res.: Atmos.*, **117**(D14)

Xu J and 6 others (2013) Seasonal and diurnal variations in aerosol concentrations at a high-altitude site on the northern boundary of Qinghai-Xizang Plateau. *Atmos. Res.*, **120–121**, 240–248

Xu JZ and 5 others (2015) Chemical composition and size distribution of summertime PM2.5 at a high altitude remote location in the northeast of the Qinghai-Xizang (Tibet) Plateau: insights into aerosol sources and processing in free troposphere. *Atmos. Chem. Phys.*, **15**(9), 5069–5081

Yan F and 9 others (2016) Concentration, sources and light absorption characteristics of dissolved organic carbon on a typical glacier, the northeastern Tibetan Plateau. *Cryosphere*, **10**(6), 2611–2621

Zhang Y and 7 others (2010) Characteristics and sources of chromophoric dissolved organic matter in lakes of the Yungui Plateau, China, differing in trophic state and altitude. *Limnol. Oceanogr.*, **55**(6), 2645–2659

Zhang Y, Liu S, Shangguan D, Li J and Zhao J (2012) Thinning and Shrinkage of Laohugou no. 12 Glacier in the Western Qilian Mountains, China, from 1957 to 2007. *J. Mt. Sci.*, **9**(3), 343–350

Zhao JH (2012) Research on UV/TiO_2 photocatalytic oxidation of organic matter in drinking water and its influencing factors. *Procedia Environ. Sci.*, **580–583**(Part A), 2358–2362

Zhou Y and 5 others (2015) Lake Taihu, a large, shallow and eutrophic aquatic ecosystem in China serves as a sink for chromophoric dissolved organic matter. *J. Great Lakes Res.*, **41**(2), 597–606

https://doi.org/10.1017/aog.2018.20 Published online by Cambridge University Press